Journal of Engineering Science and Technology
Vol. 11, No. 10 (2016) 1450 - 1469

ENHANCING THE STABILITY OF UNMANNED GROUND SPORT UTILITY VEHICLES THROUGH COORDINATED CONTROL UNDER MU-SPLIT AND GUST OF WIND

FITRI YAKUB*, YASUCHIKA MORI

Department of Intelligent Mechanical Systems, Graduate School of System Design, Tokyo Metropolitan University, Hino, 191-0065, Tokyo, Japan
*Corresponding Author: mfitri.kl@utm.my

Abstract

This study describes a comparative study of steering and yaw moment control manoeuvres in model predictive control (MPC) and linear quadratic control approaches for path following unmanned vehicles for different control manoeuvres: two-wheel steering, four-wheel steering, and direct yaw moment control. We then propose MPC with a proportional-integral (PI) controller for the coordination of active front steering (AFS) and active braking system, which particularly highlights direct yaw moment control (DYC) manoeuvres. Based on the known trajectory, we tested a vehicle at middle forward speed with the disturbance consideration of the road surface adhesion and the wind for a double lane change scenario in order to follow the desired trajectory as close as possible, minimizing tracking errors, and enhancing vehicle stability and drivability. We compared two different controllers; i) MPC with PI of an AFS and, ii) MPC with PI for coordination of AFS and DYC. The operation of the proposed integrated control is demonstrated in a Matlab simulation environment by manoeuvring the vehicle along the desired trajectory. Simulation results showed that the proposed method had yielded better tracking performances, and were able to enhance the vehicle's stability at a given speed even under road surface coefficient and wind.

Keywords: Unmanned ground vehicle, Model predictive control, Proportional-integral controller, Path following control, Road surface, Wind gust.

1. Introduction

Mathematical models of the real systems are required for the design, analysing, and development of new techniques in most engineering disciplines. Rapid development

Nomenclatures

a_y	Vehicle lateral acceleration, m s^{-2}
$b_{\phi f}$, $b_{\phi r}$	Damping coefficient of the front and rear suspension, Nm $radian^{-1}$ s^{-1}
b_w	Driveline damping coefficient, Nms
C_f, C_r	Cornering stiffness of the front and rear axle, N $radian^{-1}$
e_y	Lateral position error of the vehicle's centre of gravity to the centre line of the lane, m
e_ψ	Vehicle yaw angle error with respect to the road, radian
F_x, F_y	Longitudinal and lateral forces, N
F_w	Force exerted by a side wind, N
F_z	Vertical tire force, N
g,	Acceleration due to gravity, ms^{-2}
h	Height of the centre of gravity, m
$h_{uf,}$ h_{ur}	front and rear roll centre distances below sprung mass CoG, m
J_b	Moment of inertia of the wheel, kgm^2
$k_{\phi f}$, $k_{\phi r}$	Stiffness coefficient of the front and rear suspension, Nm $radian^{-1}$
k_{ss}	Steady-state steering angle
l	Vehicle wheelbase length, m
l_f, l_r	Distance from the centre of gravity to the front and rear axle, m
I_{xx}, I_{zz}, I_{xz}	Roll, yaw, roll-yaw moments of inertia, kgm^2
m, m_s	Total vehicle mass and sprung mass, kg
m_{uf},, m_{ur}	Front and rear unsprung mass, kg
M_w	Moment exerted by a side wind, Nm
M_z^*	The total corrective reaction moment from the DYC, Nm
r	Reference trajectory
R_w	Circular road of radius, m
r_w	Radius of the wheel, m
T_b	Wheel torque, Nm
t_w	Width of the track for front and rear vehicle, m
v_x, v_y	Longitudinal and lateral wheels velocities, ms^{-1}
v_w	Crosswind speed, ms^{-1}
x, y, z	Corresponds to the coordinates body frame of a car position

Greek Symbols

α_f, α_r	Front and rear wheels slip angles, radian
β	Vehicle side slip angle, radian
δ_f, δ_r	Steering angle of the front and rear wheels directly manipulated by the driver, radian
δ_f^*	Steering angle of the front wheel generated by the AFS, radian
κ	Path curvature
μ	Track friction coefficient
ϕ, $\dot{\phi}$	Roll and roll rate angle, radian, radian s^{-1}
ψ, $\dot{\psi}$	Vehicle heading angle and yaw rate, radian, radian s^{-1}
ω_w	Angular velocity of the tires, radian s^{-1}

Abbreviations

ABS	Anti-lock Braking System

AFS	Active Front Steering
ARS	Active Rear Steering
DoF	Degree of Freedom
DYC	Direct Yaw Moment Control
LQC	Linear Quadratic Control
MPC	Model Predictive Control
PI	Proportional Integral
SUV	Sport Utility Vehicle
2WS	Two-Wheel Steering
4WS	Four-Wheel Steering

of technology in control software offers the opportunity and chances to implement more advanced control theory towards applications.

In spite of that, model predictive control (MPC) is an optimal model based control algorithm that has been intensely investigated by the academia and industry since its commercialization in early 1980s [1-2]. It has been widely employed which relates to automotive systems for various active safety and driver assistance systems, vehicle dynamics systems, and autonomous driving and collision avoidance systems, in order to improve the vehicle stability, ride comfort, and to prevent traffic accidents [3-5].

There have been many studies of different control manoeuvres, such as two-wheel steering (2WS) using front or rear wheels [6-7], four-wheel steering (4WS) using front and rear wheels [8-9], and direct yaw moment control (DYC) using driving or braking forces [10-11], with different control strategies and purposes. Most previous papers have focused on the lateral and yaw dynamics models, neglecting the roll dynamic model. By including the roll dynamics in the system, we can evaluate the effectiveness of controllers, especially under high speed conditions. For this study, we limit the path following control of an unmanned ground vehicle that is related to the author's work and emphasizes that we assume a known trajectory for the lateral position and yaw angle based on the reference in [12]. We assume that the crosswind effect with road adhesion coefficient on the system, then, we compare the performance for two different controllers: MPC and linear quadratic control (LQC) based on a simple yaw-lateral two degree of freedom (2DoF) bicycle model.

Next, we propose the MPC with a proportional-integral (PI) controller in order to follow the desired trajectory as close as possible, minimizing the tracking errors, and to enhance the vehicle's stability under consideration of the road surface adhesion and the wind. We tested the car at a middle forward speed in a lateral manoeuvre for a sport utility vehicle (SUV) based on [13] which performed a double lane change. Active front steering (AFS) has a great influence on lateral vehicle behaviour under normal driving conditions [14-15], however, based on the fact that AFS is no longer able to produce enough lateral force during high acceleration because of the highly nonlinear characteristic of its tires, active braking system (ABS) is utilized to overcome this drawback for limited handling conditions [16]. We utilize ABS which focuses on DYC which produces the corrective yaw moment by using the rear braking forces between the left and the right side of the rear tire vehicle in order to avoid the interferences between AFS and DYC. The controller is designed based on simple linear 2DoF as called lateral-yaw model, while the vehicle model used is based on 8DoF including roll dynamic motion. We

compared the performance of the 2DoF controller in term of lateral position and yaw angle errors by using i) MPC with PI under AFS manoeuvre, and ii) MPC with PI under combination of AFS with DYC manoeuvre.

This paper is structured as follows. Section 2 formulates the full vehicle and nonlinear tire model. Control approaches of linear MPC algorithm, PI controller, and rear braking torques control concept are explained in Section 3 for an obstacle avoidance manoeuvres. The trajectory and minimizing tracking control method is validated by simulation and is then examined and discussed in Section 4. Finally, some concluding remarks and future work are given in Section 5.

2. Vehicle Model

2.1. Double-track model

Figure 1(a) illustrates the kinematics of the lateral vehicle motion in the curve scenario, while Fig. 1(b) describes the lateral position and yaw angle errors for vehicle motion with respect to the road. The longitudinal, lateral, yaw, and roll dynamic effects for a single track model based on a simplification that the right and left wheels are lumped in a single wheel at the front and rear axles are shown from the front and side view of the vehicle in Fig. 1(c) and 1(d), together with the nomenclature. We made an assumption that the slip angles at both wheels are zero, the steering angle, and the vehicle side slip angle are approximated to be too small, thus can be neglected. The front and rear suspensions are simplified by an equivalent damping and stiffness coefficients. We considered the sprung vehicle mass and the suspension and wheel weights for the unsprung mass. The pitch motion was neglected. The variable at the front and rear wheels is denoted for a lower subscripts $(\cdot)_f$ and $(\cdot)_r$. A detailed explanation may be found in [17].

Using the assumption as stated above for the motion, longitudinal, lateral, yaw, roll, and rotational dynamics of the front and rear wheels of 8DoF for the nonlinear model, vehicle motion is described in planar dynamics equations:

$$\sum F_x : m(\ddot{x} - \dot{y}\dot{\psi}) = 2F_{xf} + 2F_{xr} - m_s h\ddot{\psi}\phi - 2m_s h\dot{\psi}\dot{\phi} + (l_f - l_r)m_u\dot{\psi}^2 \tag{1}$$

$$\sum F_y : m(\ddot{y} + \dot{x}\dot{\psi}) = 2F_{yf} + 2F_{yr} + m_s h\ddot{\phi} - m_s h\phi\dot{\psi}^2 - m_s h\phi\dot{\phi}^2 + (l_r - l_f)m_u\ddot{\psi} + F_w \tag{2}$$

$$\sum M_z : I_{zz}\ddot{\psi} = 2l_f F_{yf} - 2l_r F_{yr} + {t_w}/{2}\,(-F_{xf,l} + F_{xf,r} - F_{xr,l} + F_{xr,r}) + I_{xz}\ddot{\phi} + (l_r - l_f)m_u(\ddot{y} + \dot{x}\dot{\psi}) + M_w \tag{3}$$

$$\sum M_x : (I_{xx} + m_s h^2)\ddot{\phi} + m_s h(\ddot{y} + \dot{x}\dot{\psi}) - I_{xz}\ddot{\psi} = m_s gh\phi - (k_{\phi f} + k_{\phi r})\phi - (b_{\phi f} + b_{\phi r})\dot{\phi} \tag{4}$$

$$J_b\,\dot{\omega}_{wi} = -r_w F_{xi} - T_{bi} - b_w\omega_i, \;\; i = (f, r) \tag{5}$$

The motion equations for the vehicle in an inertial frame or in *Y*-*X* axis under small angle assumption of yaw angle:

$$\dot{X} = \dot{x}\cos\psi - \dot{y}\sin\psi \approx v_x - \dot{y}\psi, \qquad \dot{Y} = \dot{x}\sin\psi + \dot{y}\cos\psi \approx v_x\psi + \dot{y} \tag{6}$$

For a simple kinematic lateral motion model formulation, yaw rate can be derived from the geometric relation as shown in Fig. 1(a), considering its limitations due to the capability of the vehicle in maximum acceleration:

$$\dot{\psi}_{des} = \frac{v_x}{R_w} = \kappa v_x, \qquad R_w = \frac{v_x^2}{\mu g} \tag{7}$$

The trajectory errors of lateral and yaw vehicle motions with respect to the centre lane of the road are as shown in Fig. 1(b):

$$\dot{e}_y = \dot{y}\cos(e_\psi) + \dot{x}\sin(e_\psi), \qquad e_\psi = \psi - \psi_{des} \tag{8}$$

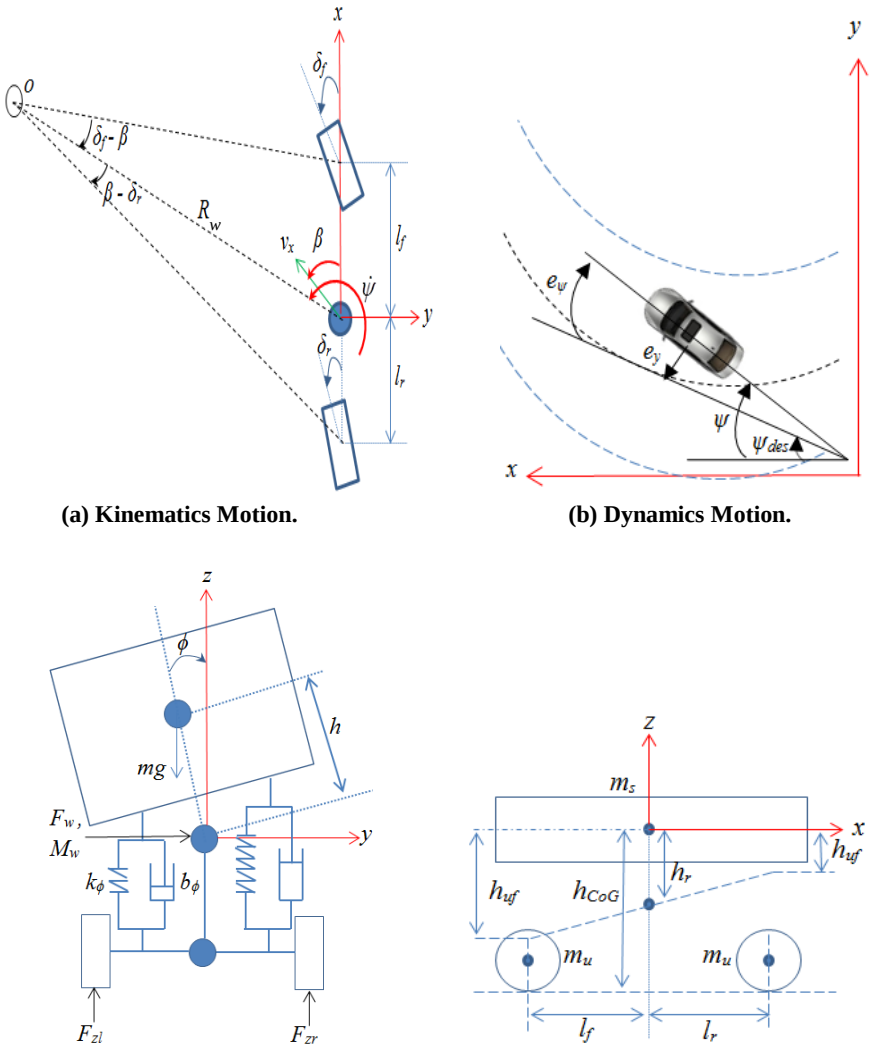

(a) Kinematics Motion. **(b) Dynamics Motion.**

(c) Front View. **(d) Side View.**

Fig. 1. SUV dynamics model.

2.2. Nonlinear tire model

In this study, we used a semi-empirical tire model [18] where the nonlinear characteristic of the longitudinal and lateral forces on the front and rear tires are characterized and modelled as:

$$F_x(s) = D_x \sin\left[C_x \tan^{-1}\left\{B_x(1-E_x)s + E_x \tan^{-1}(B_x s)\right\}\right], \tag{9}$$

$$F_y(\alpha) = D_y \sin\left[C_y \tan^{-1}\left\{B_y(1-E_y)\alpha + E_y \tan^{-1}(B_y \alpha)\right\}\right], \tag{10}$$

where parameter *B*, *C*, *D*, and *E* are the values for stiffness factor, shape factor, peak value, and curvature factor, respectively. The relationship between longitudinal, lateral, and vertical load forces for front and rear wheels due to the load transfer caused by lateral accelerations are given by the following equations:

$$\sqrt{F_{xi}^2 + F_{yi}^2} \le \mu F_{zi}, \qquad i = (f, r) \tag{11}$$

$$F_{zfi} = \frac{l_r mg}{2l} - \frac{F_{yfi}\phi}{2} \mp \frac{k_{\phi fi}\phi}{t_w} \mp \frac{b_{\phi fi}\dot{\phi}}{t_w} \mp \frac{h_{uf}F_{yfi}}{t_w} \mp \frac{h_{uf}l_r mg\phi}{t_w l}, \; i = (l, r) \tag{12}$$

$$F_{zri} = \frac{l_f mg}{2l} - \frac{F_{yri}\phi}{2} \mp \frac{k_{\phi ri}\phi}{t_w} \mp \frac{b_{\phi ri}\dot{\phi}}{t_w} \mp \frac{h_{ur}F_{yri}}{t_w} \mp \frac{h_{ur}l_f mg\phi}{t_w l}, \; i = (l, r) \tag{13}$$

The nonlinear kinematics related to tire slip angles for the front and rear wheels, and the longitudinal tire slip ratio are given such that:

$$\alpha_f = \delta_f - \tan^{-1}\left(\frac{\dot{y} + l_f\dot{\psi}}{\dot{x}}\right), \qquad \alpha_r = \delta_r - \tan^{-1}\left(\frac{\dot{y} - l_r\dot{\psi}}{\dot{x}}\right) \tag{14}$$

$$s = 1 - \frac{v_x}{r_w\omega_w}, \quad \text{acceleration if } r_w\omega_w \ge v_x \tag{15}$$

$$s = \frac{r_w\omega_w}{v_x} - 1, \quad \text{braking if } r_w\omega_w \le v_x \tag{16}$$

2.3. Disturbance model

The effect of the wind on the stability of the vehicles is an important factor as a strong gust of wind from the inward or outward side may provide the extra force and torque required that helps resist the overturning forces. Here, we neglect the wind effect on longitudinal and roll motion, thus, according to [19], a side wind impacting the car at the wind velocity as v_w exerts a force and a moment, given by:

$$F_w = \frac{2.5\pi v_w^2}{2}, \qquad M_w = \left(\frac{2.5\pi}{2} - 3.3\left(\frac{\pi}{2}\right)^3\right)v_w^2 + \frac{(l_f - l_r)F_w}{2} \tag{17}$$

The nonlinear vehicle motions in Eqs. (1)-(17) can be described by the following compact differential equation assuming a certain road friction coefficient and tire slip angle values:

$$\dot{\xi} = f_{\mu,\alpha}(\xi, u, \omega_d, r), \qquad \eta = h(\xi) \tag{18}$$

where the state, input, disturbance, reference, and output vectors are given as:

$$\begin{aligned} &\xi = [v_y \; Y \; X \; \psi \; \dot{\psi} \; \dot{\phi} \; \phi \; \omega_{fl} \; \omega_{fr} \; \omega_{rl} \; \omega_{rr}]^T, \quad u = [\delta_f \; M_z]^T \\ &\omega_d = [F_w \; M_w]^T, \quad r = [Y_{des} \; \psi_{des}]^T, \quad h(\xi) = [Y \; \psi \; \dot{\psi} \; a_y \; F_y]^T \end{aligned} \tag{19}$$

3. Coordinated Control Approach

3.1 Model Predictive Control

Model predictive control was designed based on 2DoF lateral-yaw motion by linearizing the equations from the vehicle and tire model as follows:

$$m\dot{v}_y = \frac{1}{v_x}[-\mu(C_r + C_f)v_y + (\mu(C_r l_r - C_f l_f) - m v_x^2)\dot{\psi}] + \mu C_f \delta_f + F_w \tag{20}$$

$$I_{zz}\ddot{\psi} = \frac{1}{v_x}[\mu(C_r l_r - C_f l_f)\, v_y - \mu(C_f l_f^{\,2} + C_r l_r^{\,2})\dot{\psi}] + \mu C_f l_f \delta_f + M_z + M_w \tag{21}$$

The lateral dynamics of the vehicle with AFS and DYC from the vehicle motions in Eqs. (20)-(21) can be described as follows:

$$\dot{x}_l = A_l x_l + B_{l1}u_{l1} + B_{l2}u_{l2} + B_{l3}\omega_{ld} + B_{l4}r_l \;, \qquad y_l = C_l x_l + D_l u_l \tag{22}$$

where

$$x_l = [v_y \; Y \; \dot{\psi} \; \psi]^T, \; u_{l1} = [\delta_f]^T, \; u_{l2} = [\delta_f^* \; M_z^*]^T, \; \omega_{ld} = [F_w \; M_w]^T, \; r_l = [Y_{des} \; \psi_{des}]^T, \; y_l = [Y \; \psi]^T \tag{23}$$

$x_l \in \mathrm{R}^x$, $u_l \in \mathrm{R}^u$, $\omega_{ld} \in \mathrm{R}^\omega$, $r_l \in \mathrm{R}^r$, and $y_l \in \mathrm{R}^y$ represent the state vectors, control input vectors, crosswind effects as a disturbance vectors, desired trajectory vectors, and measured output vectors, respectively.

As the MPC is designed based on a mathematical model of the plant in discrete-time, we discretized the vehicle dynamics in Eq. (22) by neglecting an unmeasured disturbance to obtain:

$$x_l(k+1|k) = A_l x_l(k|k) + B_{l1,2} u_l(k|k) + B_{l4} r_l(k|k), \qquad y_l(k|k) = C_l x_l(k|k) + D_l u_l(k|k) \tag{24}$$

where $x_l(k|k)$ is the state vector at time step k, $x_l(k + 1|k)$ is the state vector at time step k +1, with $x_l(k|k) \in \mathrm{R}^{x(k|k)}$, $u_l(k|k) \in \mathrm{R}^{u(k|k)}$, $r_l(k|k) \in \mathrm{R}^{r(k|k)}$, and $y_l(k|k) \in \mathrm{R}^{y(k|k)}$ represent the state vectors, control input vectors, reference vectors, and measured output vectors, respectively.

The controller is designed based on a linear model making it impossible for the controller to track and follow a given trajectory perfectly. The controller is designed to achieve the aim in order to follow a given trajectory, thus the objective of the predictive control system is to bring the predicted output as close as possible to the reference signal within a predictive horizon, where we assume that the reference signal remains constant in the optimization window. In other words, the objective is to find the optimal control input vector $\Delta\tilde{u}_l(k + i|k)$ such that an error function between the predicted output and the reference signal is

minimized. The optimization of the predictive control system will be solved by minimizing the cost function given by:

$$J(x_l(k),U_{lk}) = \sum_{i=1}^{H_p} \left\| \tilde{y}_l(k+i\,|\,k) - r_l(k+i\,|\,k) \right\|_{Q_i}^2 + \sum_{i=0}^{H_c-1} \left\| \Delta\tilde{u}_l(k+i\,|\,k) \right\|_{R_i}^2 \tag{25}$$

where the first summation of the cost function refers to the minimizing of the trajectory tracking error between the predicted outputs $\tilde{y}_l\,(k+i|k)$, $(i = 0,\ldots H_p - 1)$ and the output reference signal $r_l\,(k+i|k)$, $(i = 0,\ldots H_p)$. For the second summation in Eq. (25), it reflects to penalize the control signal's effort of the front steer angle or rear steer angle $\Delta\tilde{u}_l\,(k+i|k)$, $(i = 0,\ldots H_c)$ of AFS control manoeuvre. Here, $r_l\,(k+i|k)$ consists of the reference value of the lateral position and the yaw angle. The variation of the front steer angle $\Delta\tilde{u}_l\,(k+i|k)$ can be obtained when the cost function is made to be as small as possible. The weight matrix Q_i and R_i are diagonal matrices which can be adjusted for the desired closed-loop performance. We defined Q_i as the state tracking weight because the error $\tilde{y}_l\,(k+i|k) - r_l\,(k+i|k)$ can be made as small as possible by enlarging Q_i. Similarly, R_i is defined as the input tracking weight and the variation of input is reduced to make the response of the system slow by enlarging R_i. The predictive and control horizon is usually assumed to be $H_p \geq H_c$ and the control signal is assumed constant for all $H_c \leq i \leq H_p$. We formulate the optimization of the predictive control system which takes the constraints of the actuator into consideration and can be written as:

$$\begin{aligned}
&\min_{\Delta U_k} \quad J(x_l(k),\Delta U_{lk}) \\
&subject\ \ to: \\
&\quad \hat{x}_l(k+1\,|\,k) = A_l x_l(k\,|\,k) + B_{l1,2} u_l(k\,|\,k) + B_{l4}\, r_l(k|k) \\
&\quad \hat{x}_l(k+2\,|\,k) = A_l \hat{x}_l(k+1\,|\,k) + B_{l1,2} \hat{u}_l(k\,|\,k) + B_{l4}\, \hat{r}_l(k|k) \\
&\qquad\qquad \vdots \\
&\quad \hat{x}_l(k+i\,|\,k) = A_l \hat{x}_l(k+i-1\,|\,k) + B_{l1,2} \hat{u}_l(k+i-1\,|\,k) + B_{l4}\, \hat{r}_l(k+i-1\,|\,k) \\
&\quad \delta_{f,\min} \leq \hat{u}_{l1}(k+i\,|\,k) \leq \delta_{f,\max} \qquad AFS \\
&\quad \Delta\delta_{f,\min} \leq \Delta\hat{u}_{l1}(k+i\,|\,k) \leq \Delta\delta_{f,\max} \\
&\quad M_{z,\min} \leq \hat{u}_{l2}(k+i\,|\,k) \leq M_{z,\max} \qquad DYC \\
&\quad \Delta M_{z,\min} \leq \Delta\hat{u}_{l2}(k+i\,|\,k) \leq \Delta M_{z,\max}, \quad i = 1,\cdots H_p
\end{aligned} \tag{26}$$

3.2 Linear Quadratic Control

To allow a fair comparison of the tracking responses with those from MPC, the LQC is also based on the linearized vehicle Eq. (22) with a quadratic cost function. A standard 2DoF LQC tracking control structure where a feedforward controller operating on the reference is combined with a feedback controller operating on the output.

The aim of linear quadratic tracking is to track and follow the desired trajectory as close as possible, so that the tracking error is minimized but also excessive control effort is avoided with the linear quadratic solution [20]. We denote the control error by $\varepsilon_{er}(t)$, the desired trajectory by $r_l(t)$, and the performance output by $y_l(t)$, with these being related by:

$$\varepsilon_{er}(t) = r_l(t) - y_l(t) \tag{27}$$

Then, let the integral error be given by:

$$\varepsilon_e = \int_0^t \varepsilon_{er}(t)dt \tag{28}$$

which is introduced as a new state to the dynamic system in Eq. (22) as given in state-space by:

$$\begin{bmatrix} \dot{\varepsilon}_e \\ \dot{x}_l \end{bmatrix} = \begin{bmatrix} 0 & -I \\ 0 & A_l \end{bmatrix} \begin{bmatrix} \varepsilon_e \\ x_l \end{bmatrix} + \begin{bmatrix} 0 \\ B_l \end{bmatrix} u_l + \begin{bmatrix} I \\ 0 \end{bmatrix} r_l \tag{29}$$

which can be simplified as $\dot{x}_{lq} = A_{lq} x_{lq} + B_{lq} u_{lq} + E_{lq} r_l$ with obvious meaning matrices A_{lq}, B_{lq}, and E_{lq}. Thus, the new error for the system in Eq. (29) can be defined as:

$$\varepsilon = \begin{bmatrix} \varepsilon_{er} \\ \varepsilon_e \end{bmatrix} = Mr_l + Hx_{lq} \tag{30}$$

where

$$M = \begin{bmatrix} I \\ 0 \end{bmatrix}, \qquad H = \begin{bmatrix} -I & 0 \\ 0 & I \end{bmatrix} \tag{31}$$

With an infinite-horizon problem, the cost function is given by:

$$\begin{aligned} J_{lqc} &= \min_u \int_0^\infty (\varepsilon^T(t) Q_{lq} \varepsilon(t) + u_{lq}{}^T(t) R_{lq} u_{lq}(t))\, dt \\ &\textit{subject to}: \\ &\dot{\varepsilon}(t) = A_{lq}\varepsilon(t) + B_{lq}u_{lq}(t) \\ &\varepsilon(0) = \varepsilon_0 \\ &u_{lq}(t) \in U_{lq} \\ &U_{lq} = \{u_{lq} \in \Re^m \mid u_{lq\min} \le u_{lq} \le u_{lq\max}\} \end{aligned} \tag{32}$$

where Q_{lq} and R_{lq} are positive semi-definite and positive-definite weighting matrices on tracking error and input error, respectively. The value of the weighting factors must be chosen to achieve a suitable balance between error minimization and level of control effort. We try to find the control $u_{lq}(t)$ that will regulate the system at zero by tuning Q_{lq} and R_{lq}.

The set $U_{lq} \in \mathrm{R}^m$ is defined by lower and upper bounds, with u_{lqmin}, $u_{lqmax} \in \mathrm{R}^m$, $u_{lqmin} < u_{lqmax}$, where all inequalities are to be understood component wise. The optimal input state feedback controller K_{opt} is obtained by minimizing the cost function. Detailed explanation of the solution of the algebraic Riccati equation for the LQR optimal gain may be found in [21].

3.3 MPC with PI controller

The state feedback from the MPC is adopted with the PI controller to stabilize the vehicle about a known trajectory and to correct the errors that accumulated by

non-modelled vehicle dynamics, disturbances, or parameter uncertainties as shown in Fig. 2. From Fig. 2, the control signal from the PI controller given in Laplace transform as:

$$k_{pi} = k_p + \frac{k_i}{s} \tag{33}$$

where k_p and k_i are the proportional and integral gains, respectively. Let us assume the steering controller is contained by MPC and a PI controller as follows:

$$u_l(k) = -k_{mpc}^{4x1}\, x(k) + k_{pi} \tag{34}$$

From the lateral position and yaw tracking error in Eq. (8), then, by substituting Eqs. (20)-(21) into Eq. (8), it yields:

$$\begin{aligned} m\ddot{e}_y = \dot{e}_y\left[-\frac{1}{v_x}\mu C_f - \frac{1}{v_x}\mu C_r\right] + e_\psi(\mu C_f + \mu C_r) + \dot{e}_\psi\left[-\frac{1}{v_x}\mu C_f l_f + \frac{1}{v_x}\mu C_r l_r\right] \\ + \dot{\psi}_{des}\left[-\frac{1}{v_x}\mu C_f l_f + \frac{1}{v_x}\mu C_r l_r\right] + \mu C_f \delta_f + F_w \end{aligned} \tag{35}$$

$$\begin{aligned} I_{zz}\ddot{e}_\psi = \dot{e}_y\left[-\frac{1}{v_x}\mu C_f l_f + \frac{1}{v_x}\mu C_r l_r\right] + e_\psi(\mu C_f l_f - \mu C_r l_r) + \dot{e}_\psi\left[-\frac{1}{v_x}\mu C_f l_f^2 - \frac{1}{v_x}\mu C_r l_r^2\right] \\ + \dot{\psi}_{des}\left[-\frac{1}{v_x}\mu C_f l_f^2 - \frac{1}{v_x}\mu C_r l_r^2\right] - I_{zz}\ddot{\psi}_{des} + \mu C_f l_1 \delta_f + M_z + M_w \end{aligned} \tag{36}$$

The state-space model in tracking error variables, is therefore given by [22]:

$$\begin{aligned} \begin{bmatrix} \dot{e}_y \\ \ddot{e}_y \\ \dot{e}_\psi \\ \ddot{e}_\psi \end{bmatrix} &= \begin{bmatrix} 0 & 1 & 0 & 0 \\ 0 & -\frac{\mu(C_f + C_r)}{mv_x} & \frac{\mu(C_f + C_r)}{m} & -\frac{\mu(C_f l_f - C_r l_r)}{mv_x} \\ 0 & 0 & 0 & 1 \\ 0 & -\frac{\mu(C_f l_f - C_r l_r)}{I_{zz} v_x} & \frac{\mu(C_f l_f - C_r l_r)}{I_{zz}} & -\frac{\mu(C_f l_f^2 + C_r l_r^2)}{I_{zz} v_x} \end{bmatrix} \begin{bmatrix} e_y \\ \dot{e}_y \\ e_\psi \\ \dot{e}_\psi \end{bmatrix} + \begin{bmatrix} 0 & 0 \\ \frac{1}{m} & 0 \\ 0 & 0 \\ 0 & \frac{1}{I_{zz}} \end{bmatrix} \begin{bmatrix} F_w \\ M_w \end{bmatrix} \\ &+ \begin{bmatrix} 0 \\ -\frac{\mu(C_f l_f - C_r l_r)}{mv_x} - v_x \\ 0 \\ -\frac{\mu(C_f l_f^2 + C_r l_r^2)}{I_{zz} v_x} \end{bmatrix} \dot{\psi}_{des} + \begin{bmatrix} 0 & 0 \\ \frac{\mu C_f}{m} & 0 \\ 0 & 0 \\ \frac{\mu C_f l_f}{I_{zz}} & \frac{1}{I_{zz}} \end{bmatrix} \begin{bmatrix} \delta_f \\ M_z \end{bmatrix} \end{aligned} \tag{37}$$

From the system in Eq. (22), the eigenvalues of the closed-loop matrix (A_l - $B_{l1,2}k_{mpc}$) can be chosen at any correct location that is based on its design specification. Assume the longitudinal vehicle speed is constant, thus the closed-loop system in Eq. (22) is given by:

$$\dot{x}_l = (A_l - B_{l1,2}k_{mpc})\, x_l + B_{l1,2}k_{pi} + B_{l3}\omega_{ld} + B_{l4}r_l \tag{38}$$

For simplicity, we assumed zero initial conditions, and by taking the Laplace transforms (ℓ) for Eq. (38), we might find:

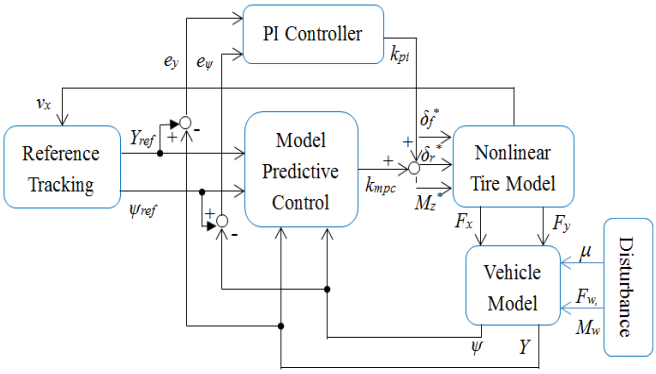

Fig. 2. Predictive Control with PI Controller Structure.

$$X_l(s) = [sI - (A_l - B_{l1,2}k_{mpc})]^{-1}\left\{B_{l1,2}\,\ell(k_{pi}) + B_{l3}\,\ell(\omega_{ld}) + B_{l4}\,\ell(r_l)\right\} \tag{39}$$

For the sake of understanding, let us assume that $r_l = \dot{\psi}_{des}$ in Eq. (7) and $\omega_{ld} = F_w$, then, for a small angle assumption, constant forward speed, and constant larger radius of curvature. So, we can get:

$$\ell(k_{pi}) = k_p + \frac{k_i}{s}, \qquad \ell(r_l) = \frac{v_x}{R_w s}, \qquad \ell(\omega_{ld}) = \frac{2.5\pi v_w^2}{2s} \tag{40}$$

Based on the final value theorem, the steady state tracking error is given by:

$$x_{ss} = \lim_{t\to\infty} x(t) = \lim_{s\to 0} s\,X_l(s) = -(A_l - B_{l1,2}k_{mpc})^{-1} \times \left[B_{l1,2}k_{ss} + B_{l3}\frac{2.5\pi v_w^2}{2s} + B_{l4}\frac{v_x}{R_w}\right] \tag{41}$$

Again, for the sake of simplicity, let us evaluate Eq. (41) by using a symbolic toolbox in Matlab, and we simplify the equation, thus yield the steady state errors:

$$x_{ss} = \begin{bmatrix} \dfrac{k_{pi}}{k_{mpc1}} - \dfrac{(l - l_r k_{mpc3})}{k_{mpc1}R_w} + \left(\dfrac{m{v_x}^2}{k_{mpc1}R_w l} - \dfrac{F_w}{k_{mpc1}l}\right)\left(\dfrac{l_f}{\mu C_r} - \dfrac{l_r}{\mu C_f} - \dfrac{l_f k_{mpc3}}{\mu C_r}\right) \\ 0 \\ \dfrac{(-\mu C_r l_f l_r - \mu C_r {l_r}^2 + l_f m{v_x}^2 + F_w R_w l_f)}{\mu C_r R_w l} \\ 0 \end{bmatrix} \tag{42}$$

If the PI steering angle is correctly chosen as in Eq. (43), the steady-state lateral position error can be made zero:

$$k_{pi} = \frac{(l - l_r k_{mpc3})}{R_w} - \left(\frac{m{v_x}^2}{R_w l} - \frac{F_w}{l}\right)\left(\frac{l_f}{\mu C_r} - \frac{l_r}{\mu C_f} - \frac{l_f k_{mpc3}}{\mu C_r}\right) \tag{43}$$

However, k_{pi} cannot influence the steady-state yaw error as seen from Eq. (42). The steady-state yaw angle error from Eq. (42) is:

$$e_{\psi ss} = \frac{m{v_x}^2 l_f}{2\mu C_r R_w l} - \frac{l_r}{R_w} \tag{44}$$

From Eq. (44), if the vehicle parameters and the vehicle speed are chosen such that:

$$\frac{l_r}{R_w} = \frac{m v_x^{\,2} l_f}{2\mu C_r R_w l} \tag{45}$$

Then, the steady-state yaw angle error of Eq. (45) can be zero. However, this only happens at one particular speed and road adhesion coefficient, and this speed and road adhesion coefficient are independent of the radius of the path.

Since the vehicle has a fixed length, both the lateral position error and yaw angle error cannot be made zero simultaneously unless the condition of Eq. (45) is satisfied. This also proved that no matter what control law is used, the yaw angle error $e_{\psi ss}$ will have the steady-state value. The vehicle slip angle is given by:

$$\beta = \arctan\left(\frac{\dot{y}}{v_x}\right) \approx \frac{1}{v_x}(\dot{e}_y - v_x e_\psi) \tag{46}$$

Since the steady-state of the lateral position error can be made zero, this gives:

$$\beta = -e_\psi = -(\psi - \psi_{des}) \tag{47}$$

Hence:

$$\beta + \psi = \psi_{des} \tag{48}$$

The main aim here is not about the steady-state error of the yaw angle but what is wanted is the heading angle of ($\beta + \psi$) to converge with the desired yaw angle.

3.4 Rear braking control

The yaw moment is controlled either by braking or engine torque through individual wheel braking. In this section, the desired direct yaw moment control M_z^* is adopted from the differences between the two sides of the vehicle torque as denoted in Eq. (5). Assume the vehicle mass is symmetric, thus, the corrective direct yaw moment can be expressed as:

$$M_z^* = \frac{t_w(F_{xr,r} - F_{xr,l})}{2} \tag{49}$$

Based on [23], the right and left wheels brake distribution is more effective than the distribution of front and rear wheels for vehicle steering manoeuvre. Thus, the corresponding torque difference between the left and right sides can be denoted in terms of M_z^* as:

$$T_{b,rl} - T_{b,rr} = \frac{2M_z^* r_w}{t_w} \tag{50}$$

In our study, the braking torque is activated only according to the e_ψ value. e_ψ is only used when the vehicle heads towards instability because of its direct effects on the longitudinal motion, while the steering angle is considered for the entire manoeuvre control. This means that we considered two control inputs; front steering angle and direct yaw moment, but only a single control input is activated

at one time. The control law is designed to select the most effective wheels to apply the brake torque, which depends on the steering condition; oversteer where the outer wheels will be selected to generate a contra-cornering yaw moment, or understeer where the inner wheels will be chosen to generate a pro-cornering yaw moment as shown in Fig. 3. It is also known that the braking at the front outside wheel and rear inside wheel is more effective to induce an understeer and oversteer yaw moment [24]. In this study, we used one wheel at a time to generate the control moment or brake torque because the vehicle has not decelerated as much as when brake torque is applied to more than one wheel to generate the same amount of yaw moment.

Thus, to avoid overlapping with the front steering angle command, only the rear wheels are involved in the control law as follows:

$$T_{b,rl}^{*} = \frac{2M_z^{*}r_w}{t_w}, \quad e_\psi < 0, \quad \dot{\psi} > 0, \qquad T_{b,rl}^{*} = \frac{2M_z^{*}r_w}{t_w}, \quad e_\psi > 0, \quad \dot{\psi} < 0 \tag{51}$$

$$T_{b,rr}^{*} = \frac{-2M_z^{*}r_w}{t_w}, \quad e_\psi < 0, \quad \dot{\psi} > 0, \qquad T_{b,rr}^{*} = \frac{-2M_z^{*}r_w}{t_w}, \quad e_\psi > 0, \quad \dot{\psi} < 0 \tag{52}$$

4. Simulation

4.1. Scenario description

The proposed methods controller, as described in Section 3.3, was implemented throughout the simulation for the path following vehicle during the double lane change scenario. In this scenario, the vehicle is considered travelling on the horizontal following the path with v_x = 20 m/s, and with road adhesion coefficient is set at μ = 0.5 (wet earth road). The drag force and torque given by Eq. (17) in the initial driving condition is assumed to act in the direction of the path at t = 1 second with v_w = 10 m/s. The forces and torques arising from this sidewise acting wind gust is assumed to be persistent and are applied as a step functions throughout the simulation time. In the first scenario, we compare MPC and LQC controllers for 2WS, 4WS, and 2WS with DYC control manoeuvres under μ = 1 and no crosswind effect with v_x = 15 m/s. Both controllers (MPC and LQC) were designed and implemented in the simulation scenarios with the parameters and conditions given in Table 1.

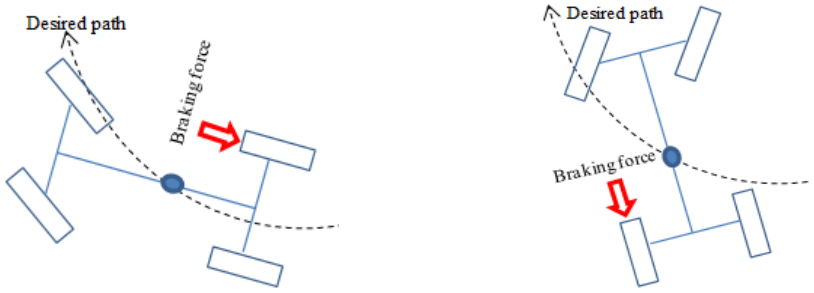

(a) Understeering **(b) Oversteering**

Fig. 3. Individual Rear Braking Wheels.

For the second scenario, we compare the effectiveness of MPC with the PI controller for AFS, and AFS with DYC control manoeuvres under the same forward speed, with crosswind effect consideration and with μ = 0.5. Table 2 illustrates the MPC with the PI controller parameters with weighting matrices that were designed and implemented in the scenarios. The weighting matrices for the inputs and outputs of MPC are selected based on trial and error from the best output responses. Simulations were performed using the Model Predictive Control Toolbox in Matlab and Simulink software within 15 seconds with a sampling time of 0.05 seconds.

Table 1. Controller Parameters for MPC and LQC.

Parameter		MPC	LQC
H_p, H_c		20, 9	20, 9
δ_f [deg]		± 20	± 20
$\Delta\delta_f$ [deg/s]		± 10	± 10
δ_r [deg]		± 20	± 20
$\Delta\delta_r$ [deg/s]		± 10	± 10
M_z [Nm]		± 1500	± 1500
ΔM_z [Nm/s]		± 1000	± 1000
R_1	2WS	0.1	5
Q_{11}, Q_{22} (v_x = 15m/s)		5.25, 0.5	20, 2.5
R_1, R_2	4WS	0.1, 0.1	5, 5
Q_{11}, Q_{22} (v_x = 15m/s)		3.95, 0.5	14.5, 2.6
R_1, R_2	2WS + DYC	0.1, 0.1	5, 5
Q_{11}, Q_{22} (v_x = 15m/s)		2.85, 0.5	10, 2.5

Table 2. Controller Parameters for MPC with PI Controller.

Parameter	AFS	AFS + DYC
H_p, H_c	20, 9	20, 11
δ_f [deg]	± 20	± 20
$\Delta\delta_f$ [deg/s]	± 10	± 10
M_z [Nm]	-	± 1500
ΔM_z [Nm/s]	-	± 1000
R_1, ΔR_1	0.1, 0.03	0.1, 0.03
R_2, ΔR_2	-	0.1, 0.03
Q_{11}, Q_{22} (v_x = 20m/s)	1.95, 0.5	2.05, 0.5
k_{p1}, k_{i1}	0.5, 0.2	0.4, 0.55
k_{p2} k_{i2}	0.25, 0.15	0.5, 0.6

4.2. Results and discussions

First, we simulated the motion of the vehicle at middle forward speed (chosen as 15 ms^{-1}) and neglected the road surface friction (which was chosen as dry concrete, μ = 1). We evaluated the MPC and LQC controllers' robustness for the output response by comparing performances of 2WS, 4WS, and 2WS with DYC manoeuvres as shown in Fig. 4. It can be seen clearly from these figures that the MPC controller, the trajectory tracking responses for lateral position and the yaw angle were similar for all control manoeuvres and it was possible to successfully track and follow a given trajectory. The lateral position responses were similar for

LQC, but it can be seen that LQC did not perform well in terms of yaw angle and yaw rate tracking responses. This shows that LQC is not suitable for control implementation in multivariable systems. Moreover, Figs. 4(b) and 4(c) illustrate that for a middle forward speed of the vehicle, the manoeuvre response was much better for 4WS and for 2WS with DYC than for 2WS. The rear steering and DYC were fully utilized in 4WS and for 2WS with DYC.

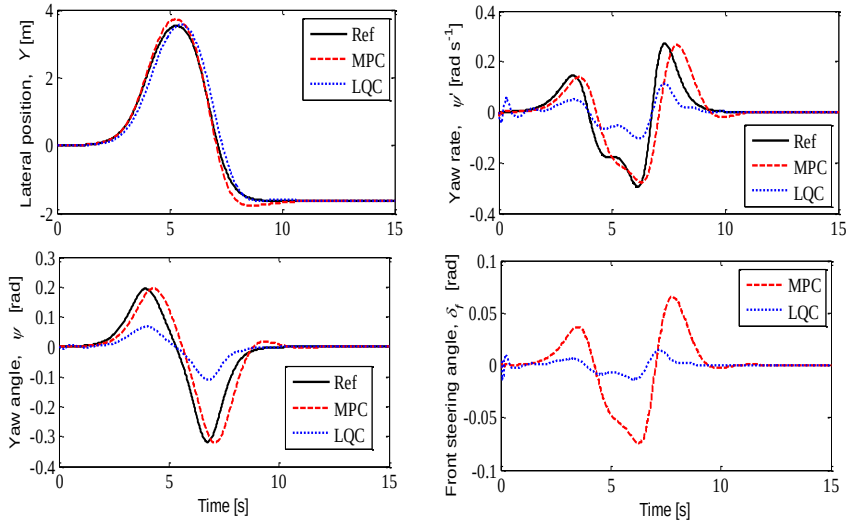

(a) 2WS

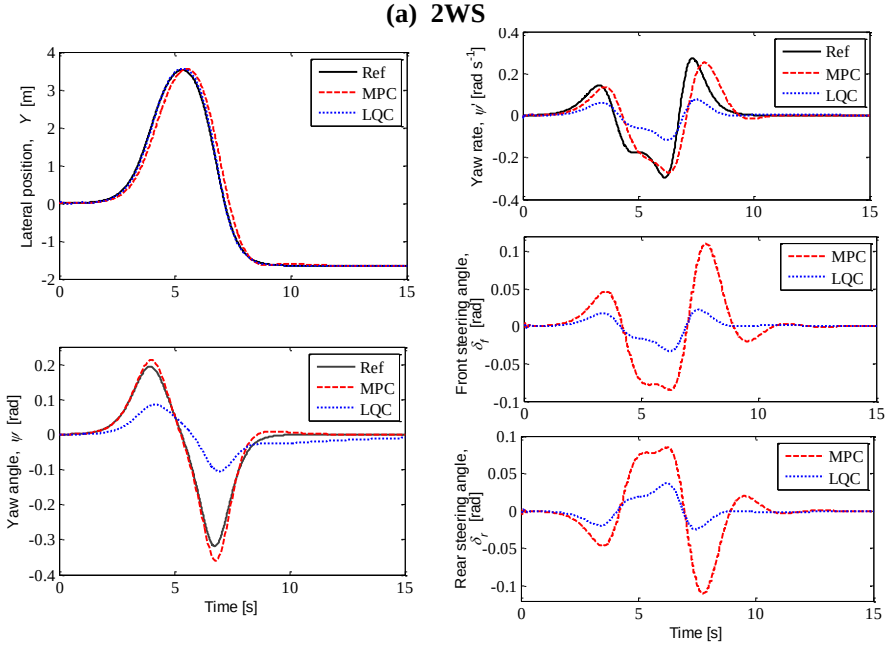

(b) 4WS

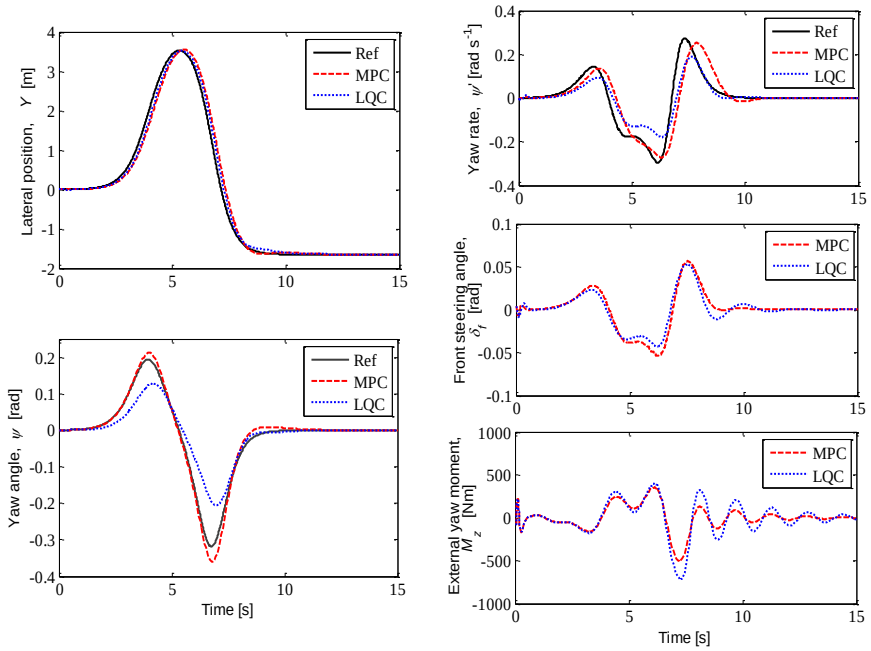

(c) 2WS + DYC

Fig. 4. Vehicle Maneuvers at 15 ms^{-1} without crosswind and μ = 1.

Next, we simulated the vehicle's behaviour at a forward speed of 20 m/s with road surface friction (wet earth road) and μ = 0.5, in a double lane change scenario to minimize tracking errors. In order to see the effectiveness of the proposed method in Sections 3.3 and 3.4, we used MPC with the PI controller and compared the results with those from AFS and AFS with DYC manoeuvres. We also compared the vehicle performances of AFS (front steer wheel with PI controller) with 2WS (front steer wheel) which was without the PI controller to evaluate the advantages of the PI controller. We compared the performance of the controller for the lateral position, yaw angle, yaw rate, lateral position error, and yaw angle error output responses as shown in Fig. 5. We like to see the effectiveness of the proposed braking control allocation as described in Section 3.4 on wet earth road under the crosswind effect.

From the Fig. 5, it can be clearly seen that AFS and AFS with DYC manoeuvres performed well in the lateral position rather than the 2WS manoeuvre. However, if we see the vehicle's responses of lateral error, we might notice that the AFS with DYC manoeuvre can minimize the lateral position errors more than the AFS manoeuvre. In the vehicle's yaw angle and yaw rate responses, both manoeuvres (2WS and AFS) cannot follow a given trajectory as close as possible, which saw 2WS perform worse than the AFS manoeuvre. However, it can be seen that the AFS with DYC manoeuvre provided a much better yaw angle and yaw rate tracking responses than the AFS manoeuvre, especially as indicated in the yaw angle error response. It shows that, by adding one more control input to the system, particularly in this case we added the direct yaw moment control as shown in Fig. 6, may enhance vehicle stability and handing even though under the disturbances of crosswind and road adhesion.

From Fig. 5, it proved that the proposed braking control algorithm was successful to enhance the vehicle stability through yaw angle and yaw rate responses.

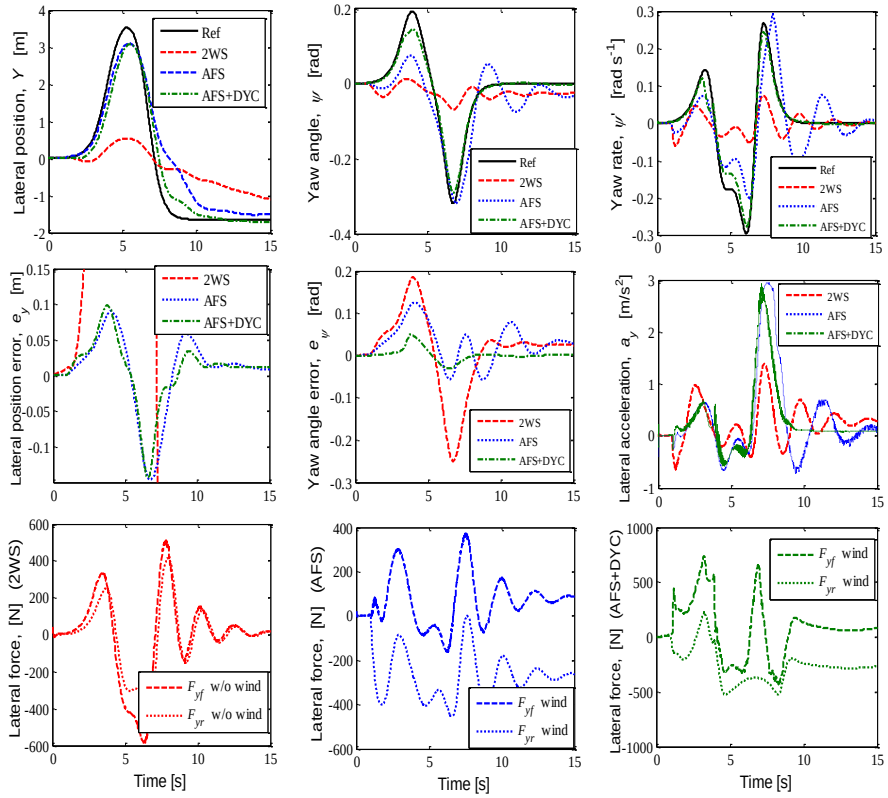

Fig. 5. Vehicle Travelling at 20 m/s with Crosswind on Wet Earth Road under AFS and AFS with DYC Control Manoeuvres.

Moreover, the crosswind effect on the system can be seen through the lateral forces at the front and rear wheels as shown in Fig. 5. In this scenario, the front steering angle and angle rate are within the constraints of both manoeuvres control. An AFS with DYC manoeuvre showed that the steady-state control signal ended at zero, while the AFS manoeuvre has a little steady-state error throughout the simulation time. The control signals of AFS with DYC can be seen through the front steering angle and direct yaw moment control as shown in Fig. 6. It was observed that the rear braking torque on the right wheels were used more than the left wheels to stabilize the vehicle manoeuvre control.

Furthermore, Fig. 6 illustrates the response of the driver control signal, PI controller signal, and steering angle generated by the AFS signal for all manoeuvres control. The results showed that at middle forward speed, an AFS manoeuvre is not able to stabilize the vehicle for the yaw rate response under crosswind and road adhesion disturbances. Therefore, it can be improved by adding another control input to the system such as active rear steering, braking system, or torque distribution at the front and/or rear wheels. With the

combination of AFS and DYC, rear braking torque distribution between left and right wheels may enhance the vehicle's stability. However, when the vehicle speed is increased or when the road surface coefficient becomes lower, the SUV that has a high centre of gravity becomes more difficult to control and stabilize. Therefore, a new control technique is needed to maintain the vehicle's stability while following the reference path in the above scenarios.

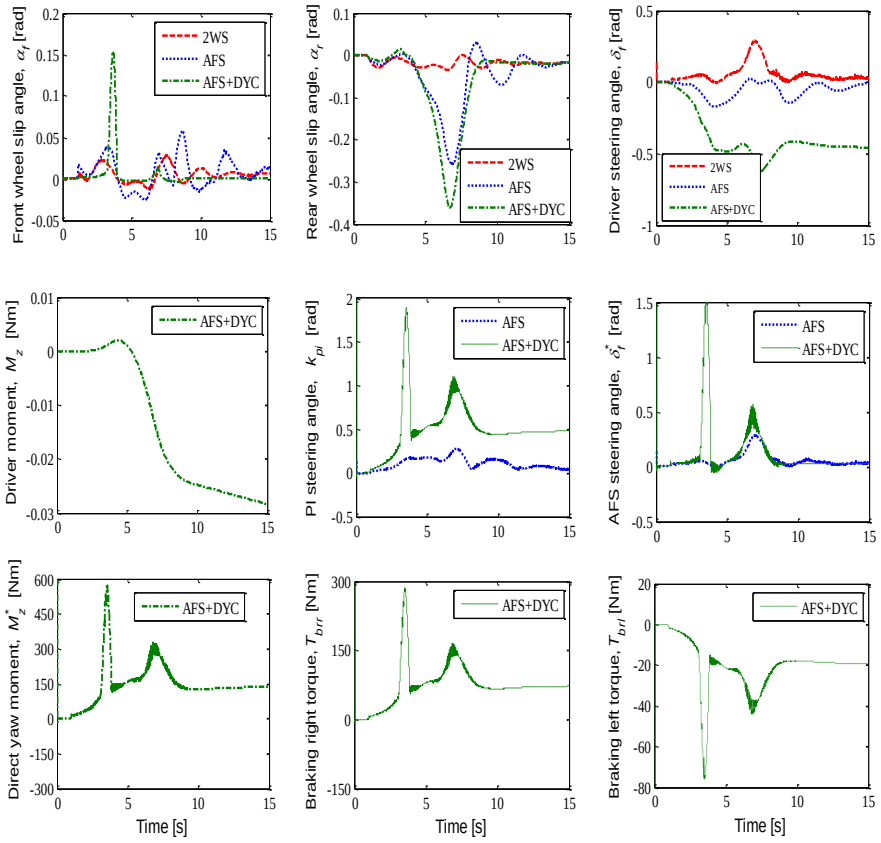

Fig. 6. Control Signal Responses Vehicle Travelling at 20 m/s with Crosswind on Wet Earth Road under AFS with DYC Control Manoeuvres.

5. Conclusions

This paper has presented a comprehensive study of MPC and LQC of an autonomous vehicle in path following control with different control manoeuvres (2WS, 4WS, and 2WS with DYC). Simulation was performed at middle forward speed in a double lane change scenario. We then proposed MPC with a PI controller focused on minimizing tracking errors under the consideration of strong wind and road surface coefficient in a double lane change scenario. The simulations proved that MPC is more successful than LQC for multivariable systems and systems with constraints. However, we have highlighted that there is a trade-off for the controllers to achieve the target for two tracking outputs with one control signal; thus, MPC is very useful when implemented for multivariable systems with constraints compared to LQC.

Moreover, this study presented an integrated control approach for AFS and DYC manoeuvre based on MPC and the PI controller in order to track and follow a given trajectory as close as possible, while minimizing the output trajectory errors. The simulation result showed that by adding the PI controller with MPC, it proved that the vehicle stability, handling, and manoeuvrability can be enhanced and the lateral position tracking can be improved for a four-wheeled SUV. The results also proved that the right and left wheels' brake distribution in DYC are more effective and successfully implemented with the combination of AFS for vehicle steering manoeuvre even under the crosswind effect and on low road adhesion coefficient to the lateral and yaw motions.

The improvement of the control method with different combinations such as active rear steering, active suspension, and braking with front and rear wheels can be considered and left for further work. The proposed method is suggested to be implemented as a real application soon.

References

1. Qin, S.J.; and Badgewell, T.A. (1997). An overview of industrial model predictive control technology. *In: Chemical Process Control - V*, 93(316), 232-256.
2. Wan, Z.; and Kothare, M.V. (2003). Efficient scheduled stabilizing model predictive control for constrained nonlinear systems. *Int. J. of Robust and Nonlinear Control*, 13(3-4), 331-346.
3. Cho, W.; Yoon, J.; Kim, J.; Hur, J.; and Yi, K. (2008). An investigation into unified chassis control scheme for optimized vehicle stability and manoeuvrability. *Vehicle System Dynamics*, 46, 87−105.
4. Barbarisi, O.; Palmieri, G.; Scala, S.; and, Glielmo, L. (2009). LTV-MPC for yaw rate control and side slip control with dynamically constrained differential braking. *European J. of Control*, 15(3-4), 468-479.
5. Guvenc, B.A.; Guvenc, L.; and Karaman, S. (2009). Robust yaw stability controller design and hardware-in-the-loop testing for a road vehicle. *IEEE Trans. Veh. Technolo.*, 58(2), 555-571.
6. Nam, K.; Oh, S.; Fujimoto, H.; and Hori, Y. (2012). Robust yaw stability control for electric vehicles based on active front steering control through a steer-by-wire system. *Int. J. of Automotive Technology*, 13(7), 1169-1176.
7. Bianchi, D.; Borri, A.; Benedetto, M.D.Di.; Gennaro, S.Di.; and Burgio, G. (2010). Adaptive integrated vehicle control using active front steering and rear torque vectoring. *Int. J. of Vehicle Autonomous Systems*, 8(2/3/4), 85-105.
8. Ackermann, J.; and Sienel, W. (1993). Robust yaw damping of cars with front and rear wheel steering. *IEEE Transactions on Control Systems Technology*, 1(1), 15-20.
9. Yoshida, H.; Shinohara, S.; and Nagai, M. (2008). Lane change steering manoeuvre using model predictive control theory. *Vehicle System Dynamics*, 46(1), 669-681.
10. Kim, W.; Kim, D.; Yi, K.; and Kim, H.J. (2012). Development of a path-tracking control system based on model predictive control using infrastructure sensors. *Vehicle System Dynamics*, 50(6), 1001-1023.

11. Abe, M.; Ohkubo, N.; and Kano, Y. (1996). A direct yaw moment control for improving limit performance of vehicle handling - comparison and cooperation with 4ws. *Vehicle System Dynamics*, 25, 3-23.
12. Yakub, F; and Mori, Y. (2015). Comparative study of autonomous path-following vehicle control via model predictive control and linear quadratic control. *J. of Automobile Engineering*, doi: 10.1177/0954407014566031.
13. Elmi, N.; Ohadis, A.; and Samadi, B. (2013). Active front-steering control of a sport utility vehicle using a robust linear quadratic regulator method, with emphasis on the roll dynamics. *J. of Automobile Engineering*, 227(12), 1636-1649.
14. Li, D.; Du, S.; and Yu, F. (2008). Integrated vehicle chassis control based on direct yaw moment, active steering and active stabilizer. *Vehicle System Dynamics*, 46, 341−351.
15. Hwang, T.; Park, K.; Heo, S.; Lee, S.; and Lee, J. (2008). Design of integrated chassis control logics for AFS and ESP. *Int. J. Automotive Technology*, 9 (1), 17−27.
16. Falcone, P.; Tseng, H.E.; Borrelli, F.; Asgari, J.; and Hrovat, D. (2008). MPC-based yaw and lateral stabilization via active front steering and braking. *Vehicle System Dynamics*, 46, 611-628.
17. Yakub, F.; Mori, Y. (2015). Enhancing path following control performance of autonomous ground vehicle through coordinated approach under disturbance effect. *IEEJ Transactions on Electronics, Information and Systems*, 135(1), 102-110.
18. Pacejka, H.B.; and Besselink, I. (2012). *Tire and Vehicle Dynamics* (3rd ed.). Oxford: Butterwort-Heinemann Ltd.
19. Keviczky, T.; Falcone, P.; Borrelli, F.; Asgari, J.; and Hrovat, D. (2006). Predictive control approach to autonomous vehicle steering. *Proc. Amer. Cont. Conf.*, MN, US, 4670-4675.
20. Groves, K.P.; Sigthorsson, D.O.; Serrani, A.; Yurkovich, S.; Bolender, M.A.; and Doman, D.B. (2005). Reference command tracking for a linearized model of an air-breathing hypersonic vehicle. *Proc. AIAA Guidance, Navigation, and Control Conference and Exhibit*, AIAA-2005-6144, San Francisco, California, 1-14.
21. Hammar, G.; and Ovtchinnikov, V. (2010). Structural intelligent platooning by a systematic LQR algorithm. Master's thesis, Royal Institute of Technology, KTH.
22. Rajamani, R. (2006). *Vehicle Dynamics and Control* (3rd ed.). New York: Springer.
23. Doumiati, M.; Sename, O.; Dugard, L.; Martinez-Molina, J.M.; Gaspar, P.; and Szabo, Z. (2013). Integrated vehicle dynamics control via coordination of active front steering and rear braking. *European J. of Control*, 19(2), 121-143.
24. Tjonnas, J.; and Johansen, T.A. (2010). Stabilization of automotive vehicles using active steering and adaptive brake control allocation. *IEEE Trans. on Control Systems Technol.*, 18(3), 545-558.